Journal of Catalysis **190,** 157–172 (2000)
doi:10.1006/jcat.1999.2739, available online at http://www.idealibrary.com on IDEAL®

γ-Al_2O_3-Supported Pt Catalysts with Extremely High Dispersions Resulting from Pt–W Interactions

Oleg S. Alexeev,* George W. Graham,† Mordecai Shelef,† and Bruce C. Gates*

*Department of Chemical Engineering and Materials Science, University of California, Davis, California 95616; and †Ford Research Laboratory, Ford Motor Co., Dearborn, Michigan 48121

Received July 29, 1999; revised October 19, 1999; accepted October 19, 1999

γ-Al_2O_3-supported catalysts were prepared from bimetallic precursors, $\{Pt[W(CO)_3(C_5H_5)]_2(PhCN)_2\}$ and $\{Pt_2W_2(CO)_6(C_5H_5)_2(PPh_3)_2\}$, as well as from a mixture of $[PtCl_2(PhCN)_2]$ and $[W(CO)_6]$, and characterized by extended X-ray absorption fine structure (EXAFS) spectroscopy and chemisorption of H_2, CO, and O_2; the samples were reduced with H_2 at 400°C for 2 h prior to most characterizations. EXAFS data show that tungsten in either of the bimetallic precursors helped to maintain the platinum in a highly dispersed form during treatment in H_2, leading to supported platinum clusters of only about 4 to 6 atoms each, on average. EXAFS spectra measured at the Pt L_{II} edge indicate substantial Pt–W contributions in samples prepared from the bimetallic precursors, but not in samples prepared from the two monometallic precursors; the Pt–W coordination numbers in the former samples were about 2 and 1, respectively, at an average Pt–W distance of 2.71 Å. W L_{III} edge EXAFS data indicate substantial W–Pt interactions in the samples prepared from the bimetallic precursors, with an average W–Pt coordination number of about 1.0 at a distance of 2.71 Å. The results are consistent with the inference that W–Pt–W (or Pt–$(W)_2$–Pt) units in the precursor were largely retained following removal of the ligands by H_2 treatment. EXAFS data also show that the Pt–W interactions in samples prepared from the bimetallic precursors were strong enough to be largely maintained even under oxidation/reduction conditions at temperatures as high as 400°C. In addition to the metal–metal contributions, the EXAFS data show substantial interactions of both tungsten and platinum with oxygen atoms of the γ-Al_2O_3 support. The platinum clusters are inferred to be stabilized in a highly dispersed state by their interactions with tungsten cations (identified by oxygen uptake data), which are held in place by interactions with surface oxygen atoms of γ-Al_2O_3 (indicated by EXAFS data). In contrast, the sample prepared from the two monometallic precursors is characterized by a lack of Pt–W interactions (as indicated by the EXAFS data) and by relatively large platinum particles. The supported platinum clusters made from bimetallic precursors are characterized by lower chemisorption of CO or of hydrogen and by low catalytic activities for toluene hydrogenation at 1 atm and 60°C, relative to the values characterizing the samples made from the monometallic precursors, which incorporated larger platinum particles. On the other hand, the catalysts containing tungsten were an order of magnitude more active than Pt/γ-Al_2O_3 for hydrogenation of crotonaldehyde to give crotyl alcohol, although these catalysts were still nonselective for this reaction. The data indicate that tungsten formed isolated microscopic islands on γ-Al_2O_3, influencing the adsorption and catalysis by platinum by its proximity to the latter. Literature data indicate that other combinations of oxophilic and noble metals on oxide supports behave similarly.

Key Words: **clusters; bimetallic clusters; Pt–W/γ-Al_2O_3; toluene hydrogenation; crotonaldehyde hydrogenation.**

INTRODUCTION

Supported bimetallic catalysts are used in large-scale applications, illustrated by naphtha reforming (1) and simultaneous removal of CO, hydrocarbons, and NO from automobile exhaust (2). Conventional preparation methods give materials with relatively large metal particles and low concentrations of bimetallic structures, which are difficult to characterize structurally because of their nonuniformity. Organometallic compounds with preformed metal–metal bonds, in contrast, offer good opportunities for preparation of catalysts with maximized bimetallic interactions and well-defined, highly dispersed structures.

We have reported the preparation and characterization of highly dispersed MgO-supported bimetallic catalysts derived from $\{Pt[W(CO)_3(C_5H_5)]_2(PhCN)_2\}$, a precursor in which Pt and W are bonded to each other (3). Extended X-ray absorption fine structure (EXAFS) data indicate that the samples incorporate isolated platinum clusters linked to small tungsten oxide-like structures anchored to the oxide support, so that the oxophilic tungsten acts like an isolated, localized support for the platinum clusters. The goal of the work described here was to investigate how supports other than MgO stabilize such highly dispersed bimetallic structures and how the nuclearity and composition of the bimetallic cluster precursor influence the catalyst structure and properties, including the Pt–W interactions. We report the preparation, characterization, and catalytic properties of γ-Al_2O_3-supported samples prepared from $\{Pt[W(CO)_3(C_5H_5)]_2(PhCN)_2\}$ and from $\{Pt_2W_2(CO)_6(C_5H_5)_2(PPh_3)_2\}$—these clusters differ from each other in the structure, nuclearity, and number of metal–metal bonds (two in the former and five in the

0021-9517/00 $35.00

latter). γ-Al_2O_3 was chosen as the support because it stably adsorbs metal carbonyl precursors (4) and thus offers the prospect of formation of intact Pt–W clusters by precursor decarbonylation. For comparison, data are reported for samples prepared from a mixture of monometallic precursors.

EXPERIMENTAL METHODS

Reagents and Materials

The syntheses of organometallic precursors and the preparations and transfers of solid samples were performed with air exclusion techniques under dry N_2, by use of Schlenk and vacuum-line techniques. Gases (N_2, H_2, and CO (Matheson, UHP grade)) were purified by passage through traps containing reduced Cu/Al_2O_3 and activated zeolite to remove traces of O_2 and H_2O, respectively. The γ-Al_2O_3 support, with a BET surface area of 100 m^2/g (determined by N_2 adsorption), was prepared as described elsewhere (4) and evacuated at 400°C prior to use. Solvents (*n*-pentane and tetrahydrofuran (99% purity, Fisher) and reactants in catalysis experiments (toluene (99% purity, Fisher) and crotonaldehyde (99% purity, Aldrich)) were dehydrated, purified by refluxing, and deoxygenated by sparging of N_2 prior to use.

Synthesis of Organometallic Precursors

The trinuclear bimetallic precursor $\{Pt[W(CO)_3(C_5H_5)]_2(PhCN)_2\}$ was prepared by a multistep synthesis, the main step of which was a reaction between $[PtCl_2(PhCN)_2]$ and $Na[W(CO)_3(C_5H_5)]\cdot 2DME$ (DME is 1,2-dimethoxyethane) in tetrahydrofuran solution at −40°C (5, 6). The resultant $\{Pt[W(CO)_3(C_5H_5)]_2(PhCN)_2\}$ was purified by recrystallization from dichloromethane and isolated as an orange powder. The tetranuclear $\{Pt_2W_2(CO)_6(C_5H_5)_2(PPh_3)_2\}$ was synthesized by subsequent reaction of $\{Pt[W(CO)_3(C_5H_5)]_2(PhCN)_2\}$ with triphenylphosphine (PPh_3) in tetrahydrofuran at 67°C as described elsewhere (5, 6). $\{Pt_2W_2(CO)_6(C_5H_5)_2(PPh_3)_2\}$ was purified by recrystallization from toluene and isolated as a brown powder. The bimetallic clusters were identified by infrared spectroscopy in the ν_{CO} region, with the spectra being in good agreement with those reported (5, 6).

Sample Preparation

Samples denoted as PtW_2/γ-Al_2O_3, Pt_2W_2/γ-Al_2O_3, and $(Pt+W)/\gamma$-Al_2O_3 were prepared by slurrying of $\{Pt[W(CO)_3(C_5H_5)]_2(PhCN)_2\}$, $\{Pt_2W_2(CO)_6(C_5H_5)_2(PPh_3)_2\}$, and the mixture of $[PtCl_2(PhCN)_2]$ and $[W(CO)_6]$, respectively, in pentane with γ-Al_2O_3 powder (aluminum oxide C, Degussa) that had been partially dehydroxylated under vacuum at 400°C. Preparation of Pt/γ-Al_2O_3 from $[PtCl_2(PhCN)_2]$ is described elsewhere (7). The amount of each precursor was chosen to give a sample containing 1 wt% Pt; in the sample made from $[PtCl_2(PhCN)_2]$ and $[W(CO)_6]$, the W/Pt atomic ratio was 2. The pentane was removed by evacuation, ensuring complete uptake of the precursor(s) by the support. Prior to characterization, each sample was treated with H_2 at 400°C to remove organic ligands. Infrared spectroscopy indicated that no residues of organic ligands remained in the samples after such treatment.

Chemisorption Measurements

An RXM-100 multifunctional catalyst testing and characterization system (Advanced Scientific Designs, Inc.) with a vacuum capability of 10^{-8} Torr was used for chemisorption measurements. The amount of hydrogen, oxygen, or CO irreversibly chemisorbed on the sample was measured as the difference between the total adsorption and the physical adsorption isotherms (two isotherms measured consecutively with 30 min evacuation between measurements). Hydrogen titration of adsorbed oxygen was also measured. The methods have been reported (3). Errors in the determination of H/Pt, O/Pt, and CO/Pt values were ±10%.

Catalytic Reaction Rate Measurements

Toluene hydrogenation was carried out at 60°C and atmospheric pressure in a Pyrex flow reactor similar to that described (3). The products were analyzed with an online gas chromatograph equipped with a flame ionization detector. Similarly, the hydrogenation of crotonaldehyde was carried out in a tubular glass flow reactor at atmospheric pressure and 60°C. Liquid crotonaldehyde was fed by an ISCO liquid metering pump (Model 260D) to a vaporization chamber, where it was mixed with H_2. The crotonaldehyde and H_2 flow rates were adjusted to give a crotonaldehyde/H_2 gas phase volume ratio of 1/10. The reactor effluent was analyzed with an online gas chromatograph equipped with a 30-m J&W DB-WAX capillary column and a flame ionization detector.

In the absence of catalyst, there was no measurable conversion of toluene or of crotonaldehyde. Reported reaction rates correspond to 2 h on stream and conversion of toluene and crotonaldehyde less than 1 and 10%, respectively, when the nearly steady-state conditions were reached. Accuracy in the determination of reaction rates, determined from differential conversions, was about ±10%.

EXAFS Spectroscopy

EXAFS experiments were performed on X-ray beamline X-11A at the National Synchrotron Light Source at Brookhaven National Laboratory, Upton, NY. The ring energy was 2.5 GeV; the ring current was 80–220 mA. $(PtW_2)/\gamma$-Al_2O_3, $(Pt_2W_2)/\gamma$-Al_2O_3, and $(Pt+W)/\gamma$-Al_2O_3 were characterized by EXAFS spectroscopy after treatment

of each sample with H_2 at 400°C and after treatment with O_2 at 200–400°C followed by treatment with H_2 at 400°C. The sample mass was chosen to give an absorbance of about 2.5 at the Pt L_{II} and at the W L_{III} absorption edges. Spectra were recorded with each sample in a cell that allowed treatment in flowing gases prior to measurements (8). Details of sample handling and treatment were essentially the same as those reported earlier (3). The EXAFS data were recorded in the transmission mode after the cell had been cooled to nearly liquid nitrogen temperature. The data were collected with a Si(111) double crystal monochromator that was detuned by 20% to minimize the effects of higher harmonics in the X-ray beam. The samples were scanned at energies near the Pt L_{II} edge (13,272.6 eV) and the W L_{III} edge (10,206.8 eV).

EXAFS DATA ANALYSIS

Because of the nearness of the Pt L_{III} edge (11,563.7 eV) to the W L_{II} edge (11,544 eV), the data analysis for the bimetallic sample was done for the W L_{III} (10, 206.8 eV) and Pt L_{II} (13,272.6 eV) edges. The method is limited because the Pt L_{II} edge is close to the Pt L_I edge (13,879.9 eV), and the difference of only 607.3 eV between the edges allowed data analysis up to a value of k (the wave vector) of about 12 $Å^{-1}$, which is sufficient for analysis of the first coordination shell only.

The EXAFS data were analyzed with experimentally and theoretically determined reference files as described elsewhere (3). The EXAFS data were extracted from the spectra with the XDAP software (9); the steps used to extract the EXAFS function are described elsewhere (3). The following specific procedures were applied.

The raw EXAFS data at the Pt L_{II} edge obtained for $(Pt+W)/\gamma$-Al_2O_3 were Fourier transformed with a k^3 weighting over the range $2.68 < k < 12.02$ $Å^{-1}$ with no phase correction. The Fourier-transformed data were then inverse transformed in the range $0.69 < r < 4.30$ Å (r is the distance from the absorber atom, in this case Pt) to isolate the major contributions from low-frequency noise. The EXAFS data analysis was done with 12 free parameters over the ranges $3.66 < k < 11.60$ $Å^{-1}$ and $0.69 < r < 4.30$ Å. The statistically justified number of free parameters, n, was about 19, as estimated from the Nyquist theorem (10, 11), $n = (2\Delta k \Delta r/\pi) + 1$, where Δk and Δr, respectively, are the k and r ranges used to fit the data.

The raw data characterizing $(Pt+W)/\gamma$-Al_2O_3 at the W L_{III} edge were analyzed with 12 free parameters over the ranges $3.74 < k < 15.0$ $Å^{-1}$ and $0.10 < r < 4.0$ Å. The statistically justified number of free parameters, estimated as described above, was about 29.

The raw EXAFS data at the Pt L_{II} edge obtained for $(PtW_2)/\gamma$-Al_2O_3 were analyzed with 16 free parameters over the ranges $3.66 < k < 11.85$ $Å^{-1}$ and $0.13 < r < 3.50$ Å. The statistically justified number of free parameters, estimated as described above, was about 19.

The raw data characterizing $(PtW_2)/\gamma$-Al_2O_3 at the W L_{III} edge were Fourier transformed over the range $3.5 < k < 15.87$ $Å^{-1}$ with no weighting or phase correction. The Fourier-transformed data were then inverse transformed in the range $0.10 < r < 3.42$ Å. The data analysis at the W L_{III} edge was done with 20 free parameters over the ranges $3.74 < k < 14.0$ $Å^{-1}$ and $0.10 < r < 3.42$ Å. The statistically justified number of free parameters, estimated as described above, was about 22.

The raw EXAFS data at the Pt L_{II} edge obtained for $(Pt_2W_2)/\gamma$-Al_2O_3 were analyzed with 16 free parameters over the ranges $3.66 < k < 11.80$ $Å^{-1}$ and $0.13 < r < 3.55$ Å. The statistically justified number of free parameters, estimated as described above, was about 19.

The raw data characterizing $(Pt_2W_2)/\gamma$-Al_2O_3 at the W L_{III} edge were Fourier transformed over the range $3.5 < k < 16.07$ $Å^{-1}$ with no weighting or phase correction. The Fourier-transformed data were inverse transformed in the range $0.11 < r < 3.42$ Å. The analysis at the W L_{III} edge was done with 20 free parameters over the ranges $3.74 < k < 14.0$ $Å^{-1}$ and $0.11 < r < 3.42$ Å. The statistically justified number of free parameters, estimated as described above, was about 22.

Data analysis was done with a difference file technique (12, 13). The approach used to analyze the data at the Pt L_{II} edge and at the W L_{III} edge was similar to that described elsewhere (3). The reliable parameters for the high-Z (Pt, W) and low-Z ($O_{support}$) contributions were determined by multiple-shell fitting in r space and in k space with application of k^1 and k^3 weighting (14). Because data were obtained at both the Pt L_{II} and W L_{III} edges, it was possible to determine some EXAFS parameters (the Pt–W distance, coordination number, and Debye–Waller factor) from the data at each edge; thus, there were opportunities to evaluate the internal consistency of the fitting results. The issues are addressed in the following section.

RESULTS

EXAFS Data

The results of the EXAFS data analysis are summarized in Tables 1–6. The estimated error bounds in Tables 1–6 represent precisions determined from statistical analysis of the data, not accuracies; estimated accuracies are also stated in these tables. Comparisons exemplifying the goodness of the fits are shown in Figs. 1 and 2 for PtW_2/γ-Al_2O_3, both in k space and in r space. The residual spectra demonstrating Pt–W (determined from Pt L_{II} edge data) and W–Pt interactions (determined from W L_{III} edge data) are shown in Figs. 1D and 2C, respectively.

The reliability of the data obtained at each edge and characterizing Pt–W interactions and the validity of the fits

TABLE 1

EXAFS Results at the Pt L_{II} Edge Characterizing the γ-Al_2O_3-Supported Sample Prepared from [$PtCl_2(PhCN)_2$] and [$W(CO)_6$] and Treated in O_2 at Various Temperatures Followed by Treatment in H_2 at 400°C for 2 h[a]

Temperature of treatment in O_2 (°C)	Pt–Pt contribution				Pt–O_s contribution				Pt–O_l contribution			
	N	R (Å)	$10^3\Delta\sigma^2$ (Å^2)	ΔE_0 (eV)	N	R (Å)	$10^3\Delta\sigma^2$ (Å^2)	ΔE_0 (eV)	N	R (Å)	$10^3\Delta\sigma^2$ (Å^2)	ΔE_0 (eV)
No treatment	8.4 ± 0.8	2.74 ± 0.01	7.3 ± 0.6	−1.4 ± 0.9	0.7 ± 0.2	2.27 ± 0.03	10.0 ± 4.7	−13.3 ± 2.6	0.3 ± 0.1	2.71 ± 0.03	10.0 ± 2.8	−17.8 ± 2.3
200	8.3 ± 0.4	2.75 ± 0.01	7.3 ± 0.5	−1.3 ± 0.3	0.7 ± 0.1	2.26 ± 0.01	10.0 ± 2.4	−16.9 ± 1.3	0.2 ± 0.1	2.79 ± 0.02	−10.0 ± 2.6	−20.0 ± 2.0
300	8.4 ± 0.2	2.74 ± 0.01	7.4 ± 0.2	−1.1 ± 0.2	0.7 ± 0.1	2.26 ± 0.01	10.0 ± 2.4	−13.0 ± 1.4	0.5 ± 0.1	2.72 ± 0.02	−7.3 ± 0.7	−5.8 ± 1.5
400	8.4 ± 0.3	2.75 ± 0.01	7.6 ± 0.3	−1.4 ± 0.3	0.7 ± 0.1	2.27 ± 0.02	10.0 ± 2.6	−12.7 ± 1.9	0.5 ± 0.1	2.74 ± 0.02	−5.8 ± 1.5	−6.0 ± 1.6

[a] Notation: N, coordination number; R, distance between absorber and backscatterer atoms; $\Delta\sigma^2$, Debye–Waller factor; ΔE_0, inner potential correction; the subscripts s and l refer to short and long, respectively. The error bounds stated here were obtained from the statistical analysis of the data; they indicate the precisions, not accuracies. Estimated accuracies: N, ±20% (M–$O_{support}$, ±30%); R, ±1%; $\Delta\sigma^2$, ±30%; ΔE_0, ±10%.

were evaluated on the basis of the goodness of the fits and the following constraints: (a) the bond distances (R) and Debye–Waller factors ($\Delta\sigma^2$) must be the same for the Pt–W and W–Pt contributions and (b) the relationship between coordination numbers for Pt–W (N_{Pt-W}) and W–Pt (N_{W-Pt}) contributions determined from Pt and W edges and the total number of Pt (n_{Pt}) and W (n_W) atoms in the sample must satisfy the following equation (3, 15):

$$\frac{N_{Pt-W}}{N_{W-Pt}} = \frac{n_W}{n_{Pt}} \quad [1]$$

The EXAFS data reported in Tables 3–6 show that regardless of the bimetallic cluster precursor used, the average Pt–W distance and Debye–Waller factor determined from the Pt L_{II} edge data agree well within the expected experimental uncertainties with the values characterizing the W–Pt contributions determined from the W L_{III} edge data. Moreover, the ratios of the coordination numbers observed for the Pt–W contribution at the Pt edge and the W–Pt contribution at the W edge (N_{Pt-W}/N_{W-Pt}) were found to be equal to about 2 and 1 for the samples prepared from {$Pt[W(CO)_3(C_5H_5)]_2(PhCN)_2$} and {$Pt_2W_2(CO)_6(C_5H_5)_2(PPh_3)_2$}, respectively; these values match the ratios of Pt to W atoms in PtW_2/γ-Al_2O_3 and Pt_2W_2/γ-Al_2O_3. Thus, EXAFS data at both the Pt L_{II} and the W L_{III} edges are consistent with the above-mentioned constraints.

TABLE 2

EXAFS Results at the W L_{III} Edge Characterizing the γ-Al_2O_3-Supported Sample Prepared from [$PtCl_2(PhCN)_2$] and [$W(CO)_6$] and Treated in O_2 at Various Temperatures Followed by Treatment in H_2 at 400°C for 2 h[a]

Temperature of treatment in O_2 (°C)	Shell	W–O contribution			
		N	R (Å)	$10^3\Delta\sigma^2$ (Å^2)	ΔE_0 (eV)
No treatment	First	1.5 ± 0.1	1.70 ± 0.01	3.7 ± 0.3	−0.4 ± 0.6
200	First	1.6 ± 0.1	1.70 ± 0.01	4.0 ± 0.7	0.3 ± 0.9
300	First	1.6 ± 0.1	1.70 ± 0.01	4.0 ± 0.7	0.3 ± 0.9
400	First	1.6 ± 0.1	1.70 ± 0.01	4.0 ± 0.7	0.3 ± 0.9
No treatment	Second	3.4 ± 0.5	2.27 ± 0.02	10.0 ± 0.7	−13.2 ± 2.2
200	Second	3.6 ± 0.6	2.24 ± 0.02	10.0 ± 2.8	−8.8 ± 4.2
300	Second	3.6 ± 0.6	2.24 ± 0.02	10.0 ± 2.8	−8.8 ± 4.2
400	Second	3.6 ± 0.6	2.24 ± 0.02	10.0 ± 2.8	−8.8 ± 4.2
No treatment	Third	6.0 ± 1.0	2.46 ± 0.02	10.0 ± 1.8	0.3 ± 2.3
200	Third	6.0 ± 1.2	2.43 ± 0.02	10.0 ± 2.9	4.6 ± 4.3
300	Third	6.0 ± 1.2	2.43 ± 0.02	10.0 ± 2.9	4.6 ± 4.3
400	Third	6.0 ± 1.2	2.43 ± 0.02	10.0 ± 2.9	4.6 ± 4.3

[a] Notation as in Table 1.

Platinum Dispersions Determined from EXAFS Data

The EXAFS data were used to estimate platinum dispersions on the basis of the relationship of the Pt–Pt first-shell coordination number of the average metal cluster or particle size and metal dispersion reported by Kip *et al.* (16); the method was illustrated earlier for Pt/γ-Al_2O_3 (7). The data, summarized in Table 7, demonstrate how the choice of precursor as well as treatment conditions affects the average platinum cluster size.

Chemisorption

The chemisorption data characterizing the catalysts of different composition, which were reduced with H_2 at 400°C, are summarized in Table 8. The amount of hydrogen or CO chemisorbed on (Pt + W)/γ-Al_2O_3 was less than might at first be expected on the basis of the platinum dispersion alone, determined from the EXAFS data (Table 7); even lower amounts of hydrogen and CO chemisorption were observed for samples prepared from the bimetallic cluster precursors. Taking into account that the platinum dispersion was nearly 100% in samples prepared from {$Pt[W(CO)_3(C_5H_5)]_2(PhCN)_2$} and from {$Pt_2W_2(CO)_6(C_5H_5)_2(PPh_3)_2$} (Table 7), we infer that the coverages of the platinum clusters by hydrogen and by CO do not exceed roughly 20% (Table 8).

TABLE 3

EXAFS Results at the Pt L_{II} Edge Characterizing the γ-Al_2O_3-Supported Sample Prepared from {Pt[W(CO)$_3$(C$_5$H$_5$)]$_2$(PhCN)$_2$} and Treated in O_2 at Various Temperatures Followed by Treatment in H_2 at 400°C for 2 h[a]

Temperature of treatment in O_2 (°C)	Pt–Pt contribution				Pt–W contribution				Pt–O_s and Pt–O_l contributions			
	N	R (Å)	$10^3\Delta\sigma^2$ (Å^2)	ΔE_0 (eV)	N	R (Å)	$10^3\Delta\sigma^2$ (Å^2)	ΔE_0 (eV)	N	R (Å)	$10^3\Delta\sigma^2$ (Å^2)	ΔE_0 (eV)
No treatment	3.0 ± 0.5	2.74 ± 0.01	3.8 ± 1.2	4.4 ± 1.2	2.0 ± 0.2	2.71 ± 0.01	3.0 ± 0.7	−19.9 ± 1.4	1.8 ± 0.1	2.15 ± 0.01	1.1 ± 0.7	5.3 ± 0.6
									2.0 ± 0.1	2.64 ± 0.02	4.0 ± 1.7	−0.9 ± 1.0
200	3.6 ± 0.2	2.74 ± 0.01	0.2 ± 0.2	8.2 ± 0.4	2.0 ± 0.1	2.71 ± 0.01	3.1 ± 0.5	−20.0 ± 0.5	1.7 ± 0.1	2.17 ± 0.01	−1.1 ± 0.2	8.2 ± 0.2
									2.4 ± 0.1	2.64 ± 0.01	1.5 ± 0.5	−0.2 ± 0.2
300	3.5 ± 0.2	2.74 ± 0.01	0.3 ± 0.4	9.0 ± 0.9	2.0 ± 0.2	2.71 ± 0.01	3.7 ± 0.7	−19.5 ± 1.5	2.6 ± 0.1	2.15 ± 0.01	−2.3 ± 0.3	−1.9 ± 0.3
									4.5 ± 0.3	2.66 ± 0.01	7.1 ± 0.8	−2.6 ± 0.5
400	4.8 ± 0.8	2.74 ± 0.01	1.7 ± 0.8	6.0 ± 0.3	2.0 ± 0.1	2.71 ± 0.01	3.3 ± 0.4	−19.9 ± 0.6	1.3 ± 0.1	2.16 ± 0.01	4.9 ± 0.2	13.1 ± 0.2
									1.8 ± 0.1	2.62 ± 0.01	0.4 ± 0.5	1.2 ± 0.4

[a] Notation as in Table 1.

Treatment of (Pt + W)/γ-Al_2O_3 with O_2 at temperatures in the range of 200–400°C followed by reduction at 400°C did not substantially change the platinum dispersion (as evidenced by EXAFS data, Table 7) or the amounts of hydrogen or CO chemisorption on platinum (Table 8).

A similar pattern was observed for (PtW_2)/γ-Al_2O_3. EXAFS (Table 7) and chemisorption (Table 8) data show that the combination of oxidation and reduction treatments did not significantly influence either the platinum dispersion or the chemisorption capacity.

In contrast, Pt_2W_2/γ-Al_2O_3 was stable in oxidation–reduction treatments only at temperatures lower than 300°C (Table 7). The oxidation treatment at 400°C resulted in increased coverage of the platinum by hydrogen and CO (Table 8), concomitant with a decreased platinum dispersion indicated by the EXAFS data (Table 7).

Oxidation States of Tungsten

The amounts of oxygen chemisorbed, in combination with hydrogen titration data, provide information about the average oxidation states of tungsten in the samples (Table 9). Only trace amounts of oxygen were adsorbed by the sample prepared from [W(CO)$_6$] that had been reduced with H_2 at 400°C; nor was there a detectable adsorption of

TABLE 4

EXAFS Results at the W L_{III} Edge Characterizing the γ-Al_2O_3-Supported Sample Prepared from {Pt[W(CO)$_3$(C$_5$H$_5$)]$_2$(PhCN)$_2$} and Treated in O_2 at Different Temperatures Followed by Treatment in H_2 at 400°C for 2 h[a]

Temperature of treatment in O_2 (°C)	Shell	W–Pt contribution				W–$O_{support}$ contributions			
		N	R (Å)	$10^3\Delta\sigma^2$ (Å^2)	ΔE_0 (eV)	N	R (Å)	$10^3\Delta\sigma^2$ (Å^2)	ΔE_0 (eV)
No treatment	First	0.9 ± 0.1	2.71 ± 0.01	3.1 ± 0.6	−0.3 ± 1.4	1.3 ± 0.1	1.71 ± 0.01	3.3 ± 0.3	−2.5 ± 0.3
200	First	0.9 ± 0.1	2.71 ± 0.01	3.2 ± 0.4	−1.0 ± 0.3	2.0 ± 0.1	1.71 ± 0.01	8.6 ± 0.2	3.7 ± 0.3
300	First	0.9 ± 0.1	2.71 ± 0.01	3.7 ± 0.1	−1.0 ± 0.5	2.1 ± 0.1	1.71 ± 0.01	7.7 ± 0.1	3.7 ± 0.1
400	First	0.9 ± 0.1	2.71 ± 0.01	3.5 ± 0.4	−1.0 ± 0.8	2.2 ± 0.1	1.71 ± 0.01	7.5 ± 0.2	3.3 ± 0.2
No treatment	Second	—	—	—	—	0.5 ± 0.1	2.26 ± 0.01	0.8 ± 0.8	−1.1 ± 1.3
200	Second	—	—	—	—	0.6 ± 0.1	2.22 ± 0.01	−1.3 ± 0.2	13.1 ± 0.4
300	Second	—	—	—	—	0.6 ± 0.1	2.21 ± 0.01	−0.5 ± 0.1	16.3 ± 0.3
400	Second	—	—	—	—	0.6 ± 0.1	2.20 ± 0.01	0.1 ± 0.4	18.8 ± 0.7
No treatment	Third	—	—	—	—	0.1 ± 0.1	3.09 ± 0.02	−10.0 ± 0.7	−14.2 ± 1.9
200	Third	—	—	—	—	0.6 ± 0.1	3.04 ± 0.01	−5.8 ± 0.2	−1.1 ± 1.0
300	Third	—	—	—	—	0.4 ± 0.1	3.02 ± 0.01	−6.6 ± 0.1	4.4 ± 0.1
400	Third	—	—	—	—	0.2 ± 0.1	3.02 ± 0.01	−7.6 ± 0.3	4.8 ± 0.7
No treatment	Fourth	—	—	—	—	—	—	—	—
200	Fourth	—	—	—	—	—	—	—	—
300	Fourth	—	—	—	—	1.2 ± 0.1	3.10 ± 0.01	10.0 ± 1.6	−1.7 ± 0.7
400	Fourth	—	—	—	—	1.2 ± 0.1	3.23 ± 0.01	10.0 ± 1.6	−11.6 ± 0.4

[a] Notation as in Table 1.

TABLE 5

EXAFS Results at the Pt L_{II} Edge Characterizing the γ-Al_2O_3-Supported Sample Prepared from $[Pt_2W_2(CO)_6(C_5H_5)_2(PPh_3)_2]$ and Treated in O_2 at Various Temperatures Followed by Treatment in H_2 at 400°C for 2 h[a]

Temperature of treatment in O_2 (°C)	Pt–Pt contribution				Pt–W contribution				Pt–O_s and Pt–O_l contributions			
	N	R (Å)	$10^3\Delta\sigma^2$ (Å^2)	ΔE_0 (eV)	N	R (Å)	$10^3\Delta\sigma^2$ (Å^2)	ΔE_0 (eV)	N	R (Å)	$10^3\Delta\sigma^2$ (Å^2)	ΔE_0 (eV)
No treatment	3.5 ± 0.2	2.74 ± 0.01	4.3 ± 0.4	3.3 ± 0.7	0.9 ± 0.1	2.71 ± 0.01	2.6 ± 0.8	−19.8 ± 1.2	3.0 ± 0.1	2.15 ± 0.01	−1.6 ± 0.1	0.2 ± 0.1
									2.0 ± 0.1	2.64 ± 0.01	−1.1 ± 0.3	0.6 ± 0.3
200	3.8 ± 0.4	2.74 ± 0.01	1.5 ± 0.6	8.4 ± 1.3	1.1 ± 0.2	2.71 ± 0.01	2.7 ± 1.0	−18.7 ± 3.2	2.7 ± 0.1	2.24 ± 0.01	10.0 ± 0.9	−14.7 ± 0.5
									2.3 ± 0.1	2.62 ± 0.02	8.4 ± 3.3	−9.9 ± 1.0
300	4.3 ± 0.7	2.74 ± 0.01	2.4 ± 1.1	5.5 ± 1.5	1.2 ± 0.3	2.71 ± 0.01	2.1 ± 1.1	−20.0 ± 3.4	2.3 ± 0.1	2.27 ± 0.01	9.5 ± 1.2	−18.0 ± 0.9
									2.2 ± 0.3	2.62 ± 0.02	8.5 ± 4.9	−9.7 ± 1.2
400	7.2 ± 0.8	2.74 ± 0.01	7.0 ± 0.8	0.7 ± 0.6	0.9 ± 0.3	2.71 ± 0.01	2.6 ± 2.2	−20.0 ± 2.7	1.1 ± 0.2	2.28 ± 0.02	10.0 ± 4.9	−20.0 ± 1.3
									0.3 ± 0.1	2.56 ± 0.02	−2.5 ± 2.8	0.1 ± 2.3

[a] Notation as in Table 1.

hydrogen after this treatment. Thus, we conclude that the average oxidation state of W in this sample after reduction at 400°C was about +6.

In contrast to the oxygen taken up in association with tungsten, the oxygen chemisorbed by platinum could be easily removed by hydrogen titration at room temperature (Table 9). Thus, we were easily able to distinguish the oxygen chemisorbed by platinum from the oxygen irreversibly consumed during oxidation of tungsten. The amount of oxygen adsorbed by tungsten was calculated as the difference between the total oxygen uptake by the sample and the amount of oxygen adsorbed by platinum, determined from hydrogen titration data. The average oxidation states of tungsten were thus found to be 5.6, 5.3, and 4.8 for $(Pt + W)/\gamma$-Al_2O_3, PtW_2/γ-Al_2O_3, and Pt_2W_2/γ-Al_2O_3 reduced at 400°C, respectively (Table 9).

Toluene Hydrogenation Catalysis

Data characterizing the performance of catalysts of various compositions are summarized in Table 10. The turnover frequency (TOF) was calculated on the basis of the platinum dispersions estimated from EXAFS data. The

TABLE 6

EXAFS Results at the W L_{III} Edge Characterizing the γ-Al_2O_3-Supported Sample Prepared from $[Pt_2W_2(CO)_6(C_5H_5)_2(PPh_3)_2]$ and Treated in O_2 at Various Temperatures Followed by Treatment in H_2 at 400°C for 2 h[a]

Temperature of treatment in O_2 (°C)	Shell	W–Pt contribution				W–$O_{support}$ contributions			
		N	R (Å)	$10^3\Delta\sigma^2$ (Å^2)	ΔE_0 (eV)	N	R (Å)	$10^3\Delta\sigma^2$ (Å^2)	ΔE_0 (eV)
No treatment	First	0.9 ± 0.1	2.71 ± 0.01	2.6 ± 0.1	5.7 ± 1.7	0.8 ± 0.1	1.71 ± 0.01	5.6 ± 0.2	4.3 ± 0.5
200	First	0.9 ± 0.1	2.71 ± 0.01	2.7 ± 0.1	5.0 ± 0.9	1.8 ± 0.1	1.71 ± 0.01	8.4 ± 0.1	4.8 ± 0.1
300	First	0.9 ± 0.1	2.71 ± 0.01	2.4 ± 0.1	5.3 ± 0.7	2.3 ± 0.1	1.71 ± 0.01	10.0 ± 0.2	4.5 ± 0.4
400	First	0.9 ± 0.1	2.71 ± 0.01	2.4 ± 0.4	4.7 ± 3.0	2.8 ± 0.3	1.72 ± 0.01	10.0 ± 0.8	0.6 ± 0.5
No treatment	Second	—	—	—	—	0.9 ± 0.1	2.12 ± 0.01	5.4 ± 0.3	−3.1 ± 0.4
200	Second	—	—	—	—	0.8 ± 0.1	2.09 ± 0.01	4.8 ± 0.2	−3.2 ± 0.3
300	Second	—	—	—	—	0.9 ± 0.1	2.05 ± 0.01	3.4 ± 0.2	3.9 ± 0.5
400	Second	—	—	—	—	1.0 ± 0.2	2.04 ± 0.01	2.7 ± 1.0	5.7 ± 2.4
No treatment	Third	—	—	—	—	0.4 ± 0.1	2.58 ± 0.01	−3.9 ± 0.3	−5.5 ± 0.8
200	Third	—	—	—	—	1.5 ± 0.1	2.62 ± 0.01	7.9 ± 0.2	−17.0 ± 0.2
300	Third	—	—	—	—	1.5 ± 0.1	2.63 ± 0.01	8.7 ± 0.4	−16.7 ± 0.4
400	Third	—	—	—	—	1.5 ± 0.1	2.68 ± 0.02	10.0 ± 1.1	−20.0 ± 1.0
No treatment	Fourth	—	—	—	—	0.2 ± 0.1	3.14 ± 0.01	−6.8 ± 0.3	0.8 ± 0.3
200	Fourth	—	—	—	—	1.4 ± 0.1	3.07 ± 0.01	0.3 ± 0.2	20.0 ± 0.6
300	Fourth	—	—	—	—	1.3 ± 0.1	3.08 ± 0.01	0.1 ± 0.2	19.8 ± 0.8
400	Fourth	—	—	—	—	1.1 ± 0.2	3.08 ± 0.02	−2.9 ± 0.6	20.0 ± 1.3

[a] Notation as in Table 1.

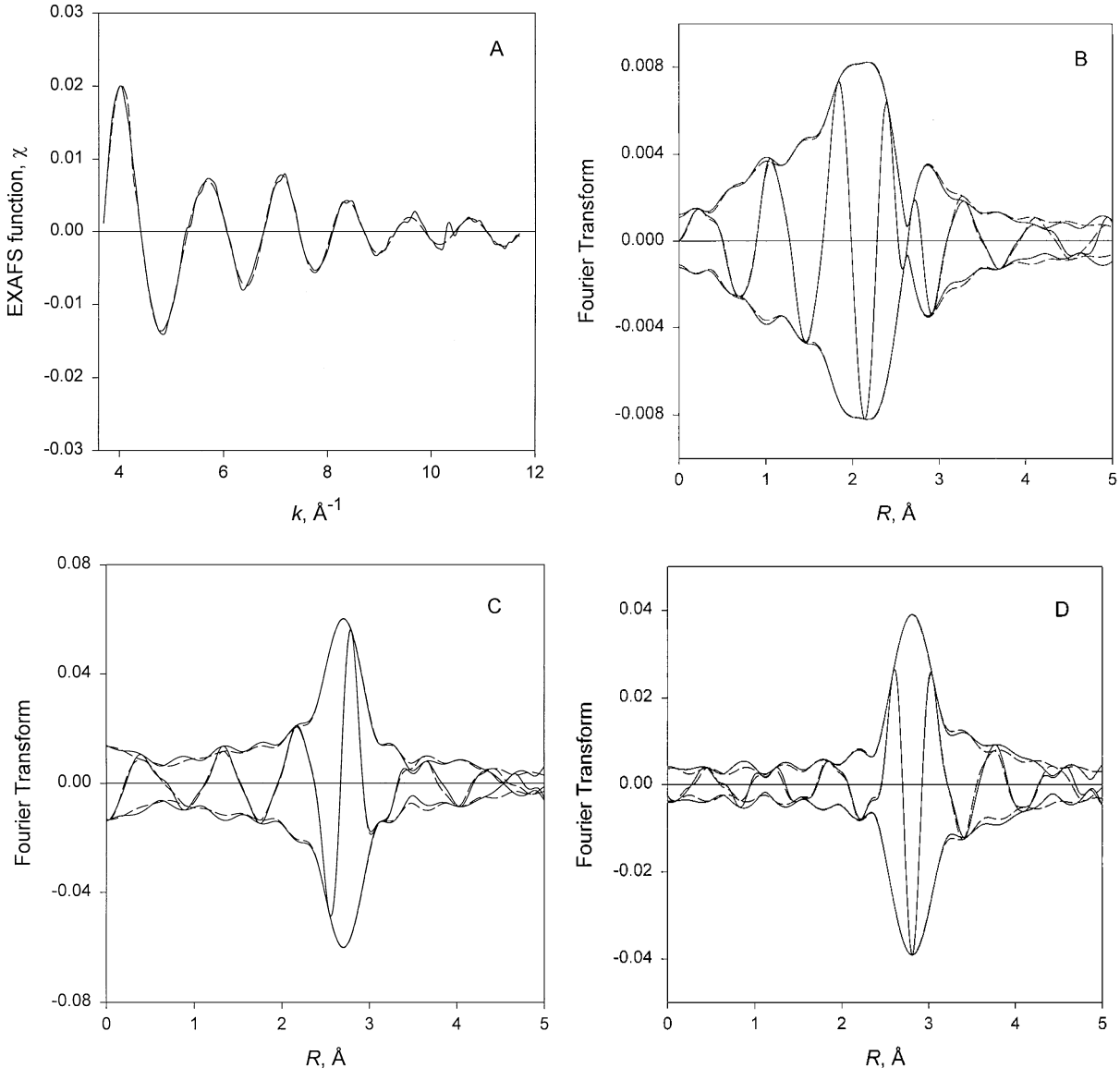

FIG. 1. Results of EXAFS analysis near the Pt L_{II} edge obtained with the best calculated coordination parameters characterizing the γ-Al_2O_3-supported sample PtW_2/γ-Al_2O_3 prepared from $\{Pt[W(CO)_3(C_5H_5)]_2(PhCN)_2\}$ following treatment in H_2 at 400°C. (A) Experimental EXAFS (solid line) and sum of the calculated Pt–Pt + Pt–O_s + Pt–O_l + Pt–W contributions (dashed line). (B) Imaginary part and magnitude of uncorrected Fourier transform (k^0 weighted) of experimental EXAFS (solid line) and sum of the calculated Pt–Pt + Pt–O_s + Pt–O_l + Pt–W contributions (dashed line). (C) Imaginary part and magnitude of phase- and amplitude-corrected Fourier transform (k^0 weighted) of raw data minus the calculated Pt–O_s + Pt–O_l + Pt–W contributions (solid line) and calculated Pt–Pt contribution (dashed line). (D) Residual spectrum illustrating the Pt–W contributions: imaginary part and magnitude of phase- and amplitude-corrected Fourier transform (k^0 weighted) of raw data minus calculated Pt–Pt + Pt–O_s + Pt–O EXAFS (solid line) and calculated Pt–W contribution (dashed line).

apparent activation energy, determined from the temperature dependence of TOF, was found to be about the same (9–11 kcal/mol) for each catalyst, in good agreement with reported values for this reaction catalyzed by supported platinum (3, 17, 18).

The TOF observed for $(Pt + W)/\gamma$-Al_2O_3 that had been reduced with H_2 at 400°C was about the same as that observed for Pt/γ-Al_2O_3 after similar treatment (Table 8). Treatment with O_2 at 400°C followed by treatment with H_2 at the same temperature did not substantially influence the catalytic behavior of either Pt/γ-Al_2O_3 or $(Pt + W)/\gamma$-Al_2O_3.

In contrast, after reduction with H_2 at 400°C, PtW_2/γ-Al_2O_3 was more than an order of magnitude less active than Pt/γ-Al_2O_3; Pt_2W_2/γ-Al_2O_3 was even less active (Table 10). After treatment with O_2 at 400°C followed by reduction at 400°C, the activity of PtW_2/γ-Al_2O_3 and that of Pt_2W_2/γ-Al_2O_3 increased; the activities were about 8 times less

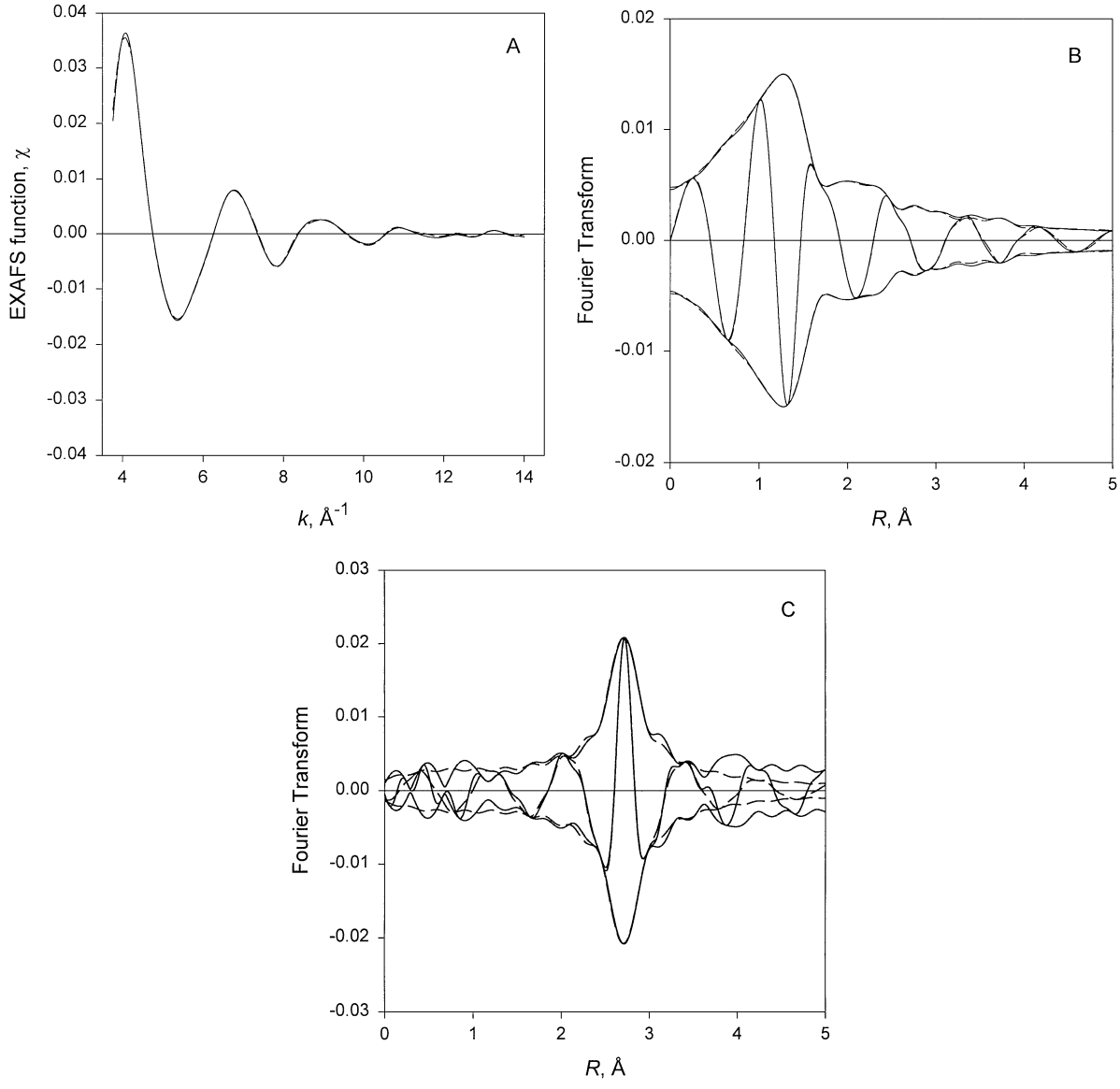

FIG. 2. Results of EXAFS analysis near the W L_{III} edge obtained with the best calculated coordination parameters characterizing the γ-Al_2O_3-supported sample PtW_2/γ-Al_2O_3 prepared from $\{Pt[W(CO)_3(C_5H_5)]_2(PhCN)_2\}$ following treatment in H_2 at 400°C. (A) Experimental EXAFS (solid line) and sum of the calculated W–$O_{support}$ + W–Pt contributions (dashed line). (B) Imaginary part and magnitude of uncorrected Fourier transform (k^0 weighted) of experimental EXAFS (solid line) and sum of the calculated W–$O_{support}$ + W–Pt contributions (dashed line). (C) Residual spectrum illustrating the W–Pt contributions: imaginary part and magnitude of phase- and amplitude-corrected Fourier transform (k^0 weighted) of raw data minus calculated W–$O_{support}$ EXAFS (solid line) and calculated W–Pt contribution (dashed line).

than that observed for Pt/γ-Al_2O_3 after similar treatment (Table 10).

Crotonaldehyde Hydrogenation Catalysis

Results characterizing catalysts of various compositions that had been reduced in H_2 at 400°C are summarized in Table 11. Butyraldehyde was the main product observed with each catalyst containing platinum when the reaction was performed at 60°C with conversions of about 10%. Besides butyraldehyde, small amounts of *n*-butane and crotyl alcohol were detected when the catalyst was Pt/γ-Al_2O_3. Tungsten increased the selectivity for formation of crotyl alcohol. The selectivity to crotyl alcohol was somewhat higher for Pt_2W_2/γ-Al_2O_3 and PtW_2/γ-Al_2O_3 than for $(Pt + W)/\gamma$-Al_2O_3, but it was generally low (Table 11). The rates of butyraldehyde, butanol, or *n*-butane formation were approximately constant and not sensitive to catalyst composition (Table 11), but the catalysts incorporating tungsten were at least an order of magnitude more active for crotyl alcohol formation than Pt/γ-Al_2O_3 (Table 11). Pt_2W_2/γ-Al_2O_3 and PtW_2/γ-Al_2O_3 were more active for crotyl alcohol formation than $(Pt + W)/\gamma$-Al_2O_3 (Table 11).

TABLE 7

Dispersions of Supported Platinum Catalysts Estimated on the Basis of EXAFS Data

Sample	Treatment	N_{Pt-Pt}[a]	Approximate average diameter of platinum clusters or particles (in metal atom diameters)[b]	Platinum cluster or particle diameter, Å	Pt_s/Pt_t[c]
$(Pt + W)/\gamma$-Al_2O_3	H_2 at 400°C	8.4	6.7	19	0.63
	O_2 at 200°C followed by H_2 at 400°C	8.3	6.5	18	0.64
	O_2 at 300°C followed by H_2 at 400°C	8.4	6.7	19	0.63
	O_2 at 400°C followed by H_2 at 400°C	8.4	6.7	19	0.63
$(PtW_2)/\gamma$-Al_2O_3	H_2 at 400°C	3.0	2.1	5.8	1.0
	O_2 at 200°C followed by H_2 at 400°C	3.6	2.6	6.9	1.0
	O_2 at 300°C followed by H_2 at 400°C	3.5	2.5	6.8	1.0
	O_2 at 400°C followed by H_2 at 400°C	4.8	3.3	9.0	1.0
$(Pt_2W_2)/\gamma$-Al_2O_3	H_2 at 400°C	3.5	2.5	6.8	1.0
	O_2 at 200°C followed by H_2 at 400°C	3.8	2.7	7.3	1.0
	O_2 at 300°C followed by H_2 at 400°C	4.3	3.0	8.3	1.0
	O_2 at 400°C followed by H_2 at 400°C	7.2	4.8	13	0.76

[a] First-shell Pt–Pt coordination number.
[b] Estimated on the basis of model reported by Kip *et al.* (16).
[c] Dispersion expressed as the ratio of the number of surface platinum atoms to total number of platinum atoms.

DISCUSSION

Evidence of Supported Pt–W Species Formed from Bimetallic Precursors

The sample made from separate monometallic precursors, $(Pt + W)/\gamma$-Al_2O_3, and reduced with H_2 at 400°C, gave a sample with EXAFS spectra at the Pt L_{II} edge showing Pt–Pt contributions but no detectable Pt–W contributions (Table 1). Consistent with this result, the W L_{III} edge data indicate W–O interactions but not W–Pt interactions (Table 2). We conclude that the platinum and tungsten components were largely segregated from each other in this sample.

TABLE 8

Influence of Treatment Conditions on Chemisorption Properties of Catalysts Reduced at 400°C

Catalyst sample	Temperature of treatment in O_2, °C[a]	Chemisorption at 25°C, atomic ratio[b]		Pt_s/Pt_t[c]	θ_H[d]	θ_{CO}[d]	Ref.
		H/Pt	CO/Pt				
Pt/γ-Al_2O_3	No treatment	0.58	0.57	0.57	1.00	1.00	7
$(Pt + W)/\gamma$-Al_2O_3	No treatment	0.47	0.55	0.63	0.75	0.87	This work
	200	0.46	0.53	0.64	0.72	0.83	
	300	0.44	0.52	0.63	0.70	0.83	
	400	0.42	0.53	0.63	0.67	0.84	
$(PtW_2)/\gamma$-Al_2O_3	No treatment	0.12	0.16	1.00	0.12	0.16	This work
	200	0.12	0.17	1.00	0.12	0.17	
	300	0.13	0.18	1.00	0.13	0.18	
	400	0.12	0.20	1.00	0.12	0.20	
$(Pt_2W_2)/\gamma$-Al_2O_3	No treatment	0.10	0.19	1.00	0.10	0.19	This work
	200	0.11	0.34	1.00	0.11	0.34	
	300	0.15	0.35	1.00	0.15	0.35	
	400	0.23	0.37	0.76	0.30	0.49	

[a] Samples were treated in 20% O_2 in He.
[b] Determined with respect to total number of Pt atoms in the sample.
[c] Dispersion (fraction of the surface atoms exposed) was estimated from EXAFS data on the basis of first-shell Pt–Pt coordination numbers using the model reported by Kip *et al.* (16).
[d] Fraction of the surface atoms covered by hydrogen or CO.

TABLE 9

Oxygen Chemisorption and Hydrogen Titration Data Characterizing γ-Al_2O_3-Supported Catalysts Reduced at 400°C

Precursor(s)	Composition, wt%	H/Pt[a]	O/Pt[b]	Hydrogen titration at 25°C[c]	O/Pt[d]	O/W[e]	N_W[f]	Ref.
$[W(CO)_6]$	2.0% W	—	—	—	—	0.05	5.9	This work
$[PtCl_2(PhCN)_2]$	1.0% Pt	0.58	0.73	1.70	0.57	—	—	7
$[PtCl_2(PhCN)_2] + [W(CO)_6]$	1.0% Pt 1.89% W	0.46	1.0	1.57	0.56	0.22	5.6	This work
$[PtW_2(CO)_6(C_5H_5)_2(PhCN)_2]$	1.0% Pt 1.89% W	0.12	1.34	1.39	0.64	0.35	5.3	This work
$[Pt_2W_2(CO)_6(C_5H_5)_2(PPh_3)_2]$	1.0% Pt 0.94% W	0.11	1.37	1.65	0.77	0.60	4.8	This work

[a] Determined after oxygen chemisorption followed by hydrogen titration and reduction of the sample at stated temperature.
[b] Total oxygen uptake determined at 200°C.
[c] Amount of hydrogen required for titration of chemisorbed oxygen, H/Pt atomic ratio.
[d] Calculated from hydrogen titration data taking into account the hydrogen chemisorption.
[e] Amount of oxygen used for oxidation of tungsten in bimetallic samples determined as the difference between the total amount of oxygen uptake and the amount of oxygen chemisorbed by platinum (determined from hydrogen titration data).
[f] Average tungsten oxidation state N_W was determined with an accuracy of about ±10% from the following equation: $N_W = 6-2(O/W)$.

In contrast, when either bimetallic precursor was used in the preparation, both Pt–Pt and Pt–W contributions were observed at the Pt L_{II} edge after reduction with H_2, and W–Pt contributions were observed at the W L_{III} edge (Tables 3–6). Thus, we infer that the bimetallic interactions of the precursors were retained to some degree in the supported catalysts and were necessary to give catalysts with substantial bimetallic interactions.

Pt–W Interactions Correspond to High Platinum Dispersions

The samples characterized by significant Pt–W interactions, PtW/γ-Al_2O_3 and Pt_2W_2/γ-Al_2O_3, have high platinum dispersions (with Pt–Pt first-shell coordination numbers of 3.0–3.5, corresponding to platinum clusters of only about 4–6 atoms each, on average (Tables 3 and 5). But $(Pt+W)/\gamma$-Al_2O_3, the sample prepared from

TABLE 10

Toluene Hydrogenation Catalyzed by γ-Al_2O_3-Supported Catalysts[a]

Catalyst	Metal content (wt%)	Treatment conditions	Pt_s/Pt_t[b]	10^2 TOF (s^{-1})	10^2 Rate per Pt atom able to chemisorb hydrogen (s^{-1})	Apparent activation energy (kcal/mol)
Pt/γ-Al_2O_3	1.0% Pt	H_2 at 400°C	0.57	16.3	16.3	10.3
		O_2 at 400°C followed by H_2 at 400°C	0.58	16.6	16.6	10.5
$(Pt+W)/\gamma$-Al_2O_3	1.0% Pt, 1.89% W	H_2 at 400°C	0.63	14.6	19.6	10.6
		O_2 at 400°C followed by H_2 at 400°C	0.63	14.9	22.4	10.9
PtW_2/γ-Al_2O_3	1.0% Pt, 1.89% W	H_2 at 400°C	1.00	0.9	7.5	10.2
		O_2 at 400°C followed by H_2 at 400°C	1.00	2.1	17.5	9.2
Pt_2W_2/γ-Al_2O_3	1.0% Pt, 0.94% W	H_2 at 400°C	1.00	0.003	0.03	10.2
		O_2 at 400°C followed by H_2 at 400°C	0.76	2.6	8.6	9.0

[a] Reaction at 60°C, $P_{toluene} = 50$ Torr and $P_{hydrogen} = 710$ Torr.
[b] Dispersion (fraction of surface Pt atoms exposed) was estimated from first-shell Pt–Pt coordination numbers by using the model reported by Kip *et al.* (16).

TABLE 11

Crotonaldehyde Hydrogenation at 60°C Catalyzed by γ-Al_2O_3-Supported Catalysts Reduced at 400°C

Catalyst	Selectivity, wt%				Activity, TOF (s^{-1})			
	butyraldehyde	butanol	crotyl alcohol	butane	butyraldehyde	butanol	crotyl alcohol	butane
Pt/γ-Al_2O_3	98.0	0.0	1.0	1.0	10.9	0.0	0.1	0.02
(Pt + W)/γ-Al_2O_3	93.6	1.0	4.1	1.3	12.7	0.3	1.0	0.48
(PtW_2)/γ-Al_2O_3	91.8	1.0	6.2	1.0	14.5	0.3	1.6	0.30
(Pt_2W_2)/γ-Al_2O_3	88.1	1.6	8.7	1.6	16.0	0.4	1.6	0.40

$[PtCl_2(PhCN)_2]$ and $[W(CO)_6]$, lacks such interactions and is characterized by a much lower platinum dispersion, with the Pt–Pt first-shell coordination number being 8.4 (Table 7). This latter value is about the same as that observed for Pt/γ-Al_2O_3 after similar treatment (7), corresponding to an average platinum particle diameter of about 19 Å, with the average particle consisting of about 90 atoms.

The first-shell Pt–O contributions, associated with the metal–support interface, provide complementary information about the metal dispersions. (Pt + W)/γ-Al_2O_3 is characterized by an average Pt–O coordination number of only 0.7, but the average Pt–O coordination numbers characterizing PtW_2/γ-Al_2O_3 and Pt_2W_2/γ-Al_2O_3 were found to be 1.8 and 3.0, respectively. Because these EXAFS parameters are averages representing all the metal atoms in the sample, the contribution of the metal–support interface to the overall EXAFS signal is expected to be minimized for the largest metal particles and maximized for the smallest. Thus, the Pt–O data are consistent with the Pt–Pt data in demonstrating the presence of relatively large platinum particles in (Pt + W)/γ-Al_2O_3 and small platinum clusters in PtW_2/γ-Al_2O_3 and Pt_2W_2/γ-Al_2O_3.

Previously it was shown that highly dispersed platinum clusters were formed on MgO when $\{Pt[W(CO)_3(C_5H_5)]_2(PhCN)_2\}$ or $\{Pt[Mo(CO)_3(C_5H_5)]_2(PhCN)_2\}$ clusters were used as precursors (3, 19); similarly, highly dispersed palladium clusters were formed on MgO from $\{Pd_2Mo_2(CO)_6(C_5H_5)_2(PPh_3)_2\}$ (20). The extremely high noble metal dispersions reported here for γ-Al_2O_3-supported Pt–W samples are in agreement with the previous reports (3, 19, 20) and lead us to infer a general conclusion: the noble metal dispersion can be maximized when bimetallic clusters containing noble and oxophilic metals bonded to each other are used as precursors in oxide-supported catalysts.

State of Tungsten in Reduced Samples

The chemisorption data (Table 9) show that when the sample was prepared from only $[W(CO)_6]$ (and reduced at 400°C) incorporated tungsten cations were in a high oxidation state (+6). The average oxidation state of tungsten in the sample prepared from $[PtCl_2(PhCN)_2]$ and $[W(CO)_6]$ was found to be 5.6; evidently, some of the tungsten ions were partially reduced as a result of the treatment in H_2 at 400°C. Even greater reduction of tungsten was observed in samples made from the bimetallic precursors: the average tungsten oxidation state was found to be 5.3 and 4.8 for the samples prepared from $\{Pt[W(CO)_3(C_5H_5)]_2(PhCN)_2\}$ and $\{Pt_2W_2(CO)_6(C_5H_5)_2(PPh_3)_2\}$, respectively, following reduction at 400°C (Table 9). We conclude that the closer the contact between the Pt and W atoms in the sample, the deeper was the reduction of the tungsten.

A similar pattern was observed for MgO-supported tungsten and molybdenum ions in the presence of platinum (3, 19). We infer that platinum activates the hydrogen for reduction of the oxophilic metal.

Influence of Oxidation–Reduction Treatments on Platinum Dispersion

The data show that the sintering of the platinum as a result of oxidation–reduction treatments depends on the Pt–W interactions. Specifics follow.

When (Pt + W)/γ-Al_2O_3 (reduced with H_2 at 400°C) was subjected to a combination of oxidation and reduction treatments at 200–400°C, neither the Pt–Pt first-shell coordination parameters nor those representing $Pt–O_{surface}$ contributions changed significantly; these results indicate a high resistance of the relatively large supported platinum particles to sintering (Tables 1 and 7). Similar results were reported for Pt/γ-Al_2O_3 (7), but the platinum dispersion in (Pt + W)/γ-Al_2O_3 was somewhat higher (0.63) than that (0.57) observed for Pt/γ-Al_2O_3 after similar treatments, which suggests (although the difference in dispersion may be within the uncertainty of the results) that the Pt–W interactions in the former helped to stabilize the platinum dispersion. However, the effect was small, consistent with the absence of Pt–W interactions in (Pt + W)/γ-Al_2O_3 indicated by the EXAFS data.

In contrast, the oxidation–reduction treatments of PtW_2/γ-Al_2O_3 led to an increase in the Pt–Pt first-shell coordination number, but only from 3.0 to 4.8. Thus, this sample is characterized by a substantial resistance to sintering of the platinum, and the platinum dispersion was higher than that of (Pt + W)/γ-Al_2O_3. The data characterizing the metal–

support interface agree with this conclusion; the Pt–$O_{surface}$ coordination number decreased from 1.8 to 1.3 as a result of the oxidation–reduction treatments (Table 3), but the change is so small that it falls within the range of experimental uncertainty. The changes in the metal–support interface were small because the degree of the sintering was small.

Larger changes were observed for Pt_2W_2/γ-Al_2O_3 than for PtW_2/γ-Al_2O_3; the Pt–Pt first-shell coordination number of the former increased from 3.5 to 4.3 as the temperature of O_2 treatment reached 300°C. The platinum dispersion of Pt_2W_2/γ-Al_2O_3 was more sensitive to the combination of O_2–H_2 treatments at high temperatures than PtW_2/γ-Al_2O_3. The Pt–Pt first-shell coordination number of the former was found to be 7.2 after the treatment with O_2 at 400°C, which indicates that platinum particles with an average diameter of about 13 Å (having about 75% of the Pt atoms on the surface) were formed as a result of the treatment (Table 7). These changes in the platinum dispersion were accompanied by substantial changes in the metal–support interface (Table 5); with increasing temperature of O_2 treatment, the average Pt–$O_{surface}$ coordination number decreased from 3.0 to 1.1 and the Pt–$O_{surface}$ distance increased from 2.15 to 2.28 Å. Notwithstanding the sintering, however, the average platinum particle size observed in Pt_2W_2/γ-Al_2O_3 even after the treatments at 400°C was smaller than that observed for $(Pt + W)/\gamma$-Al_2O_3 after reduction at 400°C.

In summary, the EXAFS parameters characterizing the Pt–Pt and Pt–$O_{surface}$ interactions confirm the high dispersion of γ-Al_2O_3-supported platinum clusters in PtW_2/γ-Al_2O_3 and in Pt_2W_2/γ-Al_2O_3. The data demonstrate not only extremely high platinum dispersions but also the high resistance of these clusters to sintering over a wide range of temperatures in oxidation–reduction treatments. We infer that the interactions between the Pt and W atoms, which were originally bonded to each other in bimetallic cluster precursors, help to stabilize the platinum dispersion under oxidation–reduction conditions.

The high resistance to sintering of the platinum clusters formed after reduction of γ-Al_2O_3-supported $\{Pt[W(CO)_3(C_5H_5)]_2(PhCN)_2\}$ and $\{Pt_2W_2(CO)_6(C_5H_5)_2(PPh_3)_2\}$ is consistent with earlier observations of high thermal stability of platinum or palladium clusters on MgO formed from platinum–tungsten and palladium–molybdenum cluster precursors (3, 20). The data characterizing the family of samples made from precursors containing a noble metal bonded to an oxophilic metal on different metal oxide supports generally indicate highly dispersed bimetallic structures that are highly resistant to sintering under high-temperature oxidation–reduction conditions.

The EXAFS data demonstrate that treatment of PtW_2/γ-Al_2O_3 and Pt_2W_2/γ-Al_2O_3 with O_2 at 200–400°C followed by reduction at 400°C did not change the Pt–W interactions substantially. After such treatments the Pt–W first-shell coordination numbers and Pt–W distances determined from Pt L_{II} edge data as well as the W–Pt first-shell coordination numbers and W–Pt distances determined from W L_{III} edge data for both samples were essentially the same as those observed after reduction of samples at 400°C when no oxygen treatment was used (Tables 3–6). The stability in the presence of O_2 of bimetallic structures formed by treatment in H_2 of MgO-supported $\{Pt[W(CO)_3(C_5H_5)]_2(PhCN)_2\}$ was observed earlier (3). The EXAFS data presented here, together with those reported (3), show that when $\{Pt[W(CO)_3(C_5H_5)]_2(PhCN)_2\}$ or $\{Pt_2W_2(CO)_6(C_5H_5)_2(PPh_3)_2\}$ was used as a precursor, with either MgO or γ-Al_2O_3 as the support, the platinum–tungsten interactions were strong and largely maintained even under oxidizing conditions. Thus, we attribute the resistance to sintering of the bimetallic samples to the noble metal–oxophilic metal interactions.

Chemisorption Properties

Simple, well-defined Pt/γ-Al_2O_3 typically chemisorbs about the same amounts of hydrogen, CO, or oxygen, and the amounts of the chemisorbed species match platinum dispersion measured by EXAFS spectroscopy (7). The chemisorption data (Table 8) indicate that the amount of hydrogen or CO chemisorbed on $(Pt + W)/\gamma$-Al_2O_3 after reduction at 400°C was somewhat less than might have been expected on the basis of the platinum dispersion (Tables 7 and 8). Even lower values of hydrogen and CO chemisorption were observed for PtW_2/γ-Al_2O_3 after reduction at 400°C, the values of H/Pt and CO/Pt being 0.12 and 0.16, respectively (Table 8). Similarly, Pt_2W_2/γ-Al_2O_3, after reduction at 400°C, showed substantially lower values of H/Pt and CO/Pt than Pt/γ-Al_2O_3, the values being as small as 0.10 and 0.19, respectively (Table 8).

Thus, the data demonstrate that incorporation of W cations decreases the amounts of hydrogen and CO chemisorption on platinum, with the reduction in chemisorption capacity being maximized for the samples in which platinum and tungsten are in close contact with each other (as evidenced by the EXAFS data). A similar decrease in hydrogen and CO chemisorption was observed for MgO-supported platinum catalysts incorporating tungsten or molybdenum cations (3, 19).

Comparisons of the chemisorption capacities with the platinum dispersion determined by EXAFS spectroscopy for PtW_2/γ-Al_2O_3 and Pt_2W_2/γ-Al_2O_3 show that the platinum coverage was always less than 20 and 50%, respectively, regardless of the temperature and treatment conditions (Table 8). Since the chemisorptive properties of platinum were hardly affected by oxygen–hydrogen treatments at different temperatures (Table 8), we conclude that possible carbon-containing deposits that might have been

left from the original CO and organic ligands had in all likelihood been removed and could not be the cause of the low capacities for chemisorption of hydrogen and CO. We infer that the platinum–tungsten interactions underlie the low platinum chemisorption capacities.

Role of Tungsten Cations in Stabilization of Platinum Dispersion

An analysis of the W–O contributions, which we identify with the metal–support interface, provides some insight into the role of tungsten cations in stabilization of the platinum dispersion, as follows. When $(Pt + W)/\gamma$-Al_2O_3 was reduced with H_2 at 400°C, only multiple W–O interactions, at average distances of 1.70, 2.27, and 2.46 Å, were indicated by the EXAFS data at the W L_{III} edge. The observation of multiple W–O contributions within the interval of bond distances from 1.7 to 2.3 Å in the first coordination shell of tungsten is typical for EXAFS spectra of tungsten oxide (WO_3) or water-containing tungsten compounds (21). Assuming that only W–O contributions observed at an average bond distance of 1.7 and 2.27 Å represent a first coordination shell of tungsten cations, we infer that each tungsten cation interacts, on average, with 4 to 5 oxygen atoms. The fact that oxidation–reduction treatments did not have a substantial influence on the EXAFS data at the W edge (Table 2) indicates that the first coordination shell around tungsten was filled with oxygen atoms, in agreement with the chemisorption data indicating a high oxidation state of the W cations. These results confirm the strongly oxophilic character of tungsten and the appropriateness of its choice as a partner for platinum in the bimetallic catalysts used in this research.

The W L_{III} edge data characterizing PtW_2/γ-Al_2O_3 after reduction at 400°C indicate the presence of multiple W–O contributions at average distances of 1.71, 2.26, and 3.09 Å. Similarly, the W L_{III} edge data characterizing Pt_2W_2/γ-Al_2O_3 after reduction at 400°C also demonstrate the presence of multiple W–O contributions (Table 6). The observation of a variety of W–O contributions is consistent with the suggestion that tungsten oxide-like structures were formed on the γ-Al_2O_3 surface of these samples.

Thus, the EXAFS data clearly show substantial interactions of W cations with the support in all the samples incorporating tungsten. We infer that in samples prepared from the bimetallic cluster precursors, the presence of oxophilic W cations in the metal–support interface (which resulted in the strong interaction of W cations with oxygen atoms of the support, on the one hand, and the existence of strong interactions between W cations and Pt atoms, on the other) helps to hold the Pt atoms in place and hinders their migration during ligand removal or oxygen–hydrogen treatments, thereby helping to maintain the platinum dispersion. This role of γ-Al_2O_3-supported W cations in stabilization of the platinum dispersion is the same as that reported earlier for MgO-supported W and Mo cations stabilizing the dispersion of platinum (3, 19) and palladium (20).

Structural Model of Oxide-Supported Noble Metal–Oxophilic Metal Catalysts

The W edge EXAFS data clearly show that the interaction of W cations in PtW_2/γ-Al_2O_3 and Pt_2W_2/γ-Al_2O_3 with oxygen atoms of the support was substantially less than that observed for $(Pt + W)/\gamma$-Al_2O_3. The surface structures in PtW_2/γ-Al_2O_3 and Pt_2W_2/γ-Al_2O_3 were evidently different from that of $(Pt + W)/\gamma$-Al_2O_3. On the basis of similar data characterizing PdMo clusters on MgO, a simplified model was postulated with oxophilic Mo cations located preferentially at the interface between the support and the Pd atoms and bonded to both oxygen of the MgO and Pd atoms in the supported clusters (19). The EXAFS data reported here support such a model and a generalization to supported clusters prepared from bimetallic precursors containing an oxophilic metal (e.g., Mo, W) and a noble metal (e.g., Pd, Pt). As the data presented here illustrate differences between the supported clusters prepared on γ-Al_2O_3 from $\{Pt[W(CO)_3(C_5H_5)]_2(PhCN)_2\}$ and from $\{Pt_2W_2(CO)_6(C_5H_5)_2(PPh_3)_2\}$, we can refine the model.

In the sample prepared from $\{Pt_2W_2(CO)_6(C_5H_5)_2(PPh_3)_2\}$ and reduced with H_2 at 400°C, each Pt atom was surrounded on average by 3 oxygen atoms (at a distance of 2.15 Å), and each W cation interacted with about 0.8 oxygen atom of the support (at a distance of 1.71 Å). On the other hand, in the sample prepared from $\{Pt[W(CO)_3(C_5H_5)]_2(PhCN)_2\}$, after the equivalent treatment, the number of oxygen atoms surrounding a Pt atom was, on average, only 1.8 (also at a distance of 2.15 Å), and each W cation interacted on average with 1.3 oxygen atoms of the support (also at a distance of 1.71 Å). Thus, in the latter sample the platinum was less strongly anchored to the γ-Al_2O_3 and the tungsten was more strongly anchored to the γ-Al_2O_3 than in the former sample. The O_2–H_2 treatments led to increased W–O contributions in both samples, but in the case of PtW_2/γ-Al_2O_3, after oxidation at 200°C, the average W–O coordination number (at a distance of 1.71 Å) increased from 1.3 to 2.0 and was not substantially changed after further treatments. In contrast, the average W–O coordination number characterizing similar contributions in Pt_2W_2/γ-Al_2O_3 gradually increased from 0.8 to 2.8 after O_2 treatments in the temperature range 200–400°C. The EXAFS data are consistent with the postulate that the bimetallic cluster frames of the bimetallic precursors were largely maintained following ligand removal by H_2 treatment. We infer that some of the metal centers became coordinatively unsaturated during this treatment, so that there was a free energy driving force for migration of Pt–W structures and organization of the metal atoms into clusters on the γ-Al_2O_3 surface with Pt atoms and W cations interacting substantially with the support. The platinum clusters

are suggested to be stabilized in a high dispersion by their interaction with W cations, which are held in place by strong bonding to the surface oxygen atoms of the γ-Al_2O_3. The relative lack of W–O contributions observed for Pt_2W_2/γ-Al_2O_3 in comparison with PtW_2/γ-Al_2O_3 suggests that a larger fraction of the surface Pt–W structures in the former sample—with less tungsten anchoring the platinum—underwent migration on the surface, resulting in the formation of relatively large platinum aggregates after treatment under the harsher conditions. Hence, increasing the amount of the oxophilic metal initially bonded to the noble metal increases the resistance of the supported noble metal to migration and aggregation on the oxide support.

Catalysis of Toluene Hydrogenation

The data show that the turnover frequency characteristic of the sample made from the mixture of platinum and tungsten monometallic precursors was only slightly less than that characterizing the monometallic sample Pt/γ-Al_2O_3 after reduction at 400°C. Oxidation and reduction cycles did not substantially change the turnover frequencies representing either Pt/γ-Al_2O_3 or $(Pt + W)/\gamma$-Al_2O_3.

The activity of PtW_2/γ-Al_2O_3 reduced at 400°C was about 15 times less than that of Pt/γ-Al_2O_3 or $(Pt + W)/\gamma$-Al_2O_3. Pt_2W_2/γ-Al_2O_3 showed negligible activity for toluene hydrogenation after reduction at 400°C. These data are in a good agreement with earlier reports showing substantial reduction of the catalytic activity of MgO-supported platinum in the presence of W or Mo cations (3, 19).

Thus, the catalytic, EXAFS, and chemisorption data reported here for γ-Al_2O_3-supported samples, together with data reported elsewhere (3, 19) for MgO-supported Pt–W and Pt–Mo samples, lead to the following generalization: regardless of the oxide support used to prepare the bimetallic catalysts, low rates of toluene hydrogenation were observed for bimetallic samples with high platinum dispersions, relatively high electron density on platinum (indicated by the infrared spectra (3, 19, 22)), and relatively low capacities for hydrogen and CO chemisorption. These effects are attributed to the interaction of the oxophilic metal cations with the noble metal in the bimetallic structures indicated by the EXAFS spectra (3, 19). The EXAFS, catalytic, and chemisorption data characterizing $(Pt + W)/\gamma$-Al_2O_3 substantiate this conclusion and show that when platinum and tungsten were largely segregated from each other there were at most small effects of tungsten on the electronic, chemisorptive, and catalytic properties of supported platinum for toluene hydrogenation.

Any of the above-mentioned effects could contribute to the low toluene hydrogenation activities of PtW_2/γ-Al_2O_3 and Pt_2W_2/γ-Al_2O_3. For example, the low concentration of hydrogen on the platinum surface during catalysis (expected on the basis of the chemisorption data) could contribute to a low rate of the rate-determining step, which is believed to be the addition of the first hydrogen atom to the aromatic ring (23), causing the catalytic reaction rate to be lower than that on the platinum particles free of bimetallic interactions. Rates of the reaction per platinum atom that is able to chemisorb hydrogen are also shown in Table 10; it may be significant that these values are more nearly constant for the series of catalysts than the turnover frequency values shown in Table 10. Furthermore, increased electron density on platinum resulting from bimetallic interactions also would be expected to slow down the presumably fast step of toluene chemisorption on platinum (23).

Oxidation at 400°C followed by reduction at 400°C led to increased activity of PtW_2/γ-Al_2O_3 and Pt_2W_2/γ-Al_2O_3. However, even after such harsh oxidation treatments, the activities of these bimetallic catalysts remained less (about 7-fold) than that of Pt/γ-Al_2O_3 or $(Pt + W)/\gamma$-Al_2O_3. One might suggest that the observed increase in catalytic activity resulting from the treatments might be associated with breakup of Pt–W structures and/or with removal of residual carbon (from the precursor ligands) from the platinum surface as a result of high-temperature O_2 treatment. However, the results reported here do not support these suggestions because the EXAFS data together with chemisorption data show that oxidation at 200–400°C did not substantially influence the Pt–W contributions or the capacity of platinum for chemisorption. Instead, we suggest that the increased catalytic activity may be related, at least in part, to the increased nuclearity of the platinum clusters resulting from oxidation at 400°C, as indicated by the EXAFS data. This suggestion is consistent with earlier reports for MgO- and γ-Al_2O_3-supported iridium clusters (24, 25) showing a strong dependence of catalytic activity for toluene hydrogenation on the cluster (or particle) size, even though toluene hydrogenation is regarded as a structure-insensitive reaction (26, 27).

In summary, the relatively low activity for toluene hydrogenation of samples made from $\{Pt[W(CO)_3(C_5H_5)]_2(PhCN)_2\}$ and from $\{Pt_2W_2(CO)_6(C_5H_5)_2(PPh_3)_2\}$ is related to the presence of strong interactions between Pt atoms and W cations, which are stable even under oxidizing conditions. Furthermore, the catalytic data reported here are consistent with literature data (28) demonstrating a trend of diminished activity of platinum for hydrocarbon conversions when the Pt atoms are in the proximity of cations of oxophilic metals.

Catalysis of Crotonaldehyde Hydrogenation

The selective hydrogenation of C=O groups in compounds incorporating C=C groups (to give unsaturated alcohols) is an important practical goal because of the importance of unsaturated alcohols in the food, cosmetics, and pharmaceutical industries. However, hydrogenations giving such products selectively, e.g., crotyl alcohol from

crotonaldehyde, are difficult. Thermodynamics favors the hydrogenation of the C=C bond, with a Gibbs free energy change of −16.9 kcal/mol vs only −7.3 kcal/mol for hydrogenation of the C=O bond (29). Selectivity in crotonaldehyde hydrogenation is influenced by the kinetics, which is influenced by the structures of adsorbed reactant on the catalyst.

The literature suggests that crotonaldehyde can be adsorbed on a metal in a di-σ_{CC} coordination (with only the C=C bond involved in chemisorption), in a di-σ_{CO} mode (with only the C=O bond involved), and in an η_4 coordination (with both bonds involved) (30, 31); the di-σ_{CO} adsorption mode favors the formation of the unsaturated alcohol. Typically, the di-σ_{CC} and η_4 coordination of crotonaldehyde are the most favored on platinum (30, 31), consistent with the formation of butyraldehyde as the principal catalytic hydrogenation product; only butyraldehyde was observed in the hydrogenation catalyzed by Pt/SiO_2 and by Pt/η-Al_2O_3, independent of the platinum crystallite size (29, 32). The catalytic data, summarized in Table 11, are consistent with literature data (29, 32) and show that butyraldehyde was the main product observed on Pt/γ-Al_2O_3 after reduction at 400°C.

The catalysts incorporating tungsten showed higher activities for formation of crotyl alcohol than the samples lacking tungsten (Table 11), but the selectivities for crotyl alcohol formation were still generally low (<9%). Among the bimetallic samples, those with the highest activities for crotyl alcohol formation were PtW_2/γ-Al_2O_3 and Pt_2W_2/γ-Al_2O_3, but some influence of the tungsten in $(Pt + W)/\gamma$-Al_2O_3 was evident in the catalytic data, even though the EXAFS data gave no evidence of Pt–W interactions; this observation indicates a substantial influence of the tungsten. We suggest that the tungsten cations closely associated with platinum atoms could participate in the chemisorption of crotonaldehyde, perhaps providing the opportunity for formation of chemisorbed species, such as those with "tilted" adsorbate that would facilitate activation of the C=O bond as a consequence of a bifunctional interaction with both Pt atoms and W cations (33).

Thus, we suggest a role of the tungsten that is similar to the roles of other added metals modifying platinum for hydrogenation of α,β-unsaturated aldehydes. For example, tin (34, 35), iron (36), and nickel (37, 38) play such a role, and the catalytic properties of Pt/TiO_2 result from high-temperature H_2 treatment; modification of the catalytic properties of Ru/SiO_2 resulting from addition of potassium promoter were also reported (32, 39).

Thus, it seems plausible to suggest that a bifunctional coordination of crotonaldehyde to both platinum and a second metal may facilitate activation of the C=O bond. Alternatively, however, there is evidence of structure sensitivity illustrated by the effects of platinum, rhodium, and ruthenium particle sizes on hydrogenation of α,β-unsaturated aldehydes (e.g., cinnamaldehyde and crotonaldehyde) (30, 40, 41). Thus, the effect of tungsten on crotonaldehyde hydrogenation may be comparable to its effect on toluene hydrogenation and may be largely a cluster size effect that reflects the extremely high platinum dispersions in the catalysts made from the bimetallic precursors.

CONCLUSIONS

Highly dispersed Pt–W structures were formed on γ-Al_2O_3 from bimetallic cluster precursors with Pt–W bonds. The bimetallic interactions were largely maintained after removal of the organic ligands from the precursors and even after treatment of the supported bimetallics under oxidizing conditions at 400°C. The interactions of W cations with oxygen atoms of the support, on the one hand, and with platinum clusters, on the other (demonstrated by EXAFS data), help to stabilize the dispersion of the platinum in clusters as small as 4 to 6 atoms each, on average, as shown by EXAFS data. Results characterizing a family of oxide-supported bimetallic catalysts made from precursors containing a noble metal bonded to an oxophilic metal generally indicate highly dispersed bimetallic structures that are highly resistant to sintering under high-temperature oxidation–reduction conditions. Increasing the amount of the tungsten initially bonded to the platinum increased the resistance of the supported platinum to migration and aggregation on the support. The resistance to aggregation is attributed to the oxophilic metal–noble metal interactions. The interaction of W cations with platinum decreases both the chemisorption capacity of the platinum clusters for hydrogen and CO and the catalytic activity for toluene hydrogenation. As the tungsten helps to stabilize the platinum in small clusters, the effects of tungsten on the chemisorption and catalytic properties are inferred to reflect, at least in part, a cluster size effect; the results parallel those for monometallic (iridium) clusters on metal oxide supports. The presence of tungsten with platinum in the catalysts leads to an increase in the rate of C=O bond hydrogenation in crotonaldehyde relative to that observed for Pt/γ-Al_2O_3, but the selectivities for this reaction are still low. The effect of tungsten on the catalytic properties of the bimetallics for crotonaldehyde hydrogenation may be attributed at least in part to the role of tungsten in maintaining the platinum in a highly dispersed state.

ACKNOWLEDGMENTS

This research was supported by the National Science Foundation (GOALI Grant CTS-9529455) and by Ford Motor Co. We acknowledge beam time and the support of the U.S. Department of Energy, Division of Materials Sciences, under Contract No. DE-FG05-89ER45384, for its role in the operation and development of beam line X-11A at the National Synchrotron Light Source. The NSLS is supported by the Department of Energy, Division of Materials Sciences and Division of Chemical Sciences,

under Contract No. DE-AC02-76CH00016. We are grateful to the staff of beam line X-11A for their assistance. The EXAFS data were analyzed with the XDAP software (9).

REFERENCES

1. "Catalytic Naphtha Reforming" G. A. Antos, A. M. Aitani, and J. M. Parera, Eds. Dekker, New York, 1995.
2. Shelef, M., and Graham, G. W., *Catal. Rev.-Sci. Eng.* **36**, 433 (1994).
3. Alexeev, O., Shelef, M., and Gates, B. C., *J. Catal.* **164**, 1 (1996).
4. Alexeev, O., Panjabi, G., and Gates, B. C., *J. Catal.* **173**, 196 (1998).
5. Bender, R., Braunstein, P., Jud, J.-M., and Dusausoy, Y., *Inorg. Chem.* **23**, 4489 (1984).
6. Braunstein, P., Bender, R., and Jud, J.-M., *Inorg. Synth.* **26**, 341 (1989).
7. Alexeev, O., Kim, D.-W., Graham, G. W., Shelef, M., and Gates, B. C., *J. Catal.* **185**, 170 (1999).
8. Jentoft, R. E., Deutsch, S. E., and Gates, B. C., *Rev. Sci. Instrum.* **67**, 2111 (1996).
9. Vaarkamp, M., Linders, J. C., and Koningsberger, D. C., *Physica B* **209**, 159 (1995).
10. Brigham, E. O., "The Fast Fourier Transform." Prentice-Hall, Englewood Cliffs, NJ, 1974.
11. Stern, E. A., *Phys. Rev. B* **48**, 9825 (1993).
12. Kirlin, P. S., van Zon, F. B. M., Koningsberger, D. C., and Gates, B. C., *J. Phys. Chem.* **94**, 8439 (1990).
13. van Zon, J. B. A. D., Koningsberger, D. C., van't Blik, H. F. J., and Sayers, D. E., *J. Chem. Phys.* **82**, 5742 (1985).
14. Koningsberger, D. C., *in* "Synchrotron Techniques in Interfacial Electrochemistry" (C. A. Melendres, and A. Tadjeddine, Eds.), p 181. Kluwer, Dordrecht, 1994.
15. Via, G. H., Drake, K. F., Meitzner, G., Lytle, F. W., and Sinfelt, J. H., *Catal. Lett.* **5**, 25 (1990).
16. Kip, B. J., Duivenvoorden, F. B. M., Koningsberger, D. C., and Prins, R., *J. Catal.* **105**, 26 (1987).
17. Lin, D. S., and Vannice, M. A., *J. Catal.* **143**, 539 (1993).
18. Lin, D. S., and Vannice, M. A., *J. Catal.* **143**, 554 (1993).
19. Alexeev, O., Kawi, S., Shelef, M., and Gates, B. C., *J. Phys. Chem.* **100**, 253 (1996).
20. Kawi, S., Alexeev, O., Shelef, M., and Gates, B. C., *J. Phys. Chem.* **99**, 6926 (1995).
21. Balerna, A., Bernieri, E., Burattini, E., Kuzmin, A., Lusis, A., Purans, J., and Cikmach, P., *Nucl. Instrum. Methods A* **308**, 234 (1991).
22. Alexeev, O., Graham, G. W., Kim, D.-W., Shelef, M., and Gates, B. C., *Phys. Chem. Chem. Phys.* **1**, 5725 (1999).
23. Lin, D. S., and Vannice, M. A., *J. Catal.* **143**, 563 (1993).
24. Xu, Z., Xiao, F.-S., Purnell, S. K., Alexeev, O., Kawi, S., Deutsch, S. E., and Gates, B. C., *Nature (London)* **372**, 346 (1994).
25. Alexeev, O., and Gates, B. C., *J. Catal.* **176**, 310 (1998).
26. Boudart, M., and Djéga-Mariadassou, G., "Kinetics of Heterogeneous Catalytic Reaction." Princeton University Press, Princeton, NJ, 1984.
27. Che, M., and Bennett, C. O., *Adv. Catal.* **36**, 55 (1989).
28. Yermakov, Yu. I., Kuznetsov, B. N., and Zakharov, V. A., "Catalysis by Supported Complexes." Elsevier, Amsterdam, 1981.
29. Vannice, M. A., *J. Mol. Catal.* **59**, 165 (1990).
30. Englisch, M., Jentys, A., and Lercher, J. A., *J. Catal.* **166**, 25 (1997).
31. Delbecq, F., and Sautet, P., *J. Catal.* **152**, 217 (1995).
32. Sen, B., and Vannice, M. A., *J. Catal.* **115**, 65 (1989).
33. Burch, R., and Flambard, A. R., *J. Catal.* **78**, 389 (1982).
34. Coloma, F., Sepúlveda-Escribano, A., Fierro, J. L. G., and Rodríguez-Reinoso, F., *Appl. Catal. A* **148**, 63 (1996).
35. Coloma, F., Sepúlveda-Escribano, A., Fierro, J. L. G., and Rodríguez-Reinoso, F., *Appl. Catal. A* **136**, 231 (1996).
36. Richard, D., Ockelford, J., Giroir-Fendler, A., and Gallezot, P., *Catal. Lett.* **3**, 53 (1989).
37. Raab, C. G., and Lercher, J. A., *J. Mol. Catal.* **75**, 71 (1992).
38. Raab, C. G., and Lercher, J. A., *Catal. Lett.* **18**, 99 (1993).
39. Waghray, A., Wang, J., Oukaci, R., and Blackmond, D. G., *J. Phys. Chem.* **96**, 5954 (1992).
40. Giroir-Fendler, A., Richard, D., and Gallezot, P., *Catal. Lett.* **5**, 175 (1990).
41. Galvagno, S., Gapannelli, G., Neri, G., Donato, A., and Pietropaolo, R., *J. Mol. Catal.* **64**, 237 (1991).